

Nanostructured Ni Coatings on Porous Alumina: Morphology, Chemical Constitution, and Cathodic Properties

R. G. Valeev^{a,*}, V. V. Stashkova^{a,b}, and A. S. Alalykin^{a,b}

^a Udmurt Federal Research Center, Ural Branch, Russian Academy of Sciences, Izhevsk, 426057 Russia

^b Udmurt State University, Izhevsk, 426034 Russia

*e-mail: rishatvaleev@mail.ru

Received August 9, 2019; revised August 9, 2019; accepted October 10, 2019

Abstract—Nanostructured nickel coatings on a well-developed surface of porous alumina offer improved performance in hydrogen evolution (cathodic) reactions owing to an increased contact area with an electrolyte. Data for the morphology, surface chemical constitution, and cathodic properties of such coatings obtained by magnetron sputtering are presented. It has been shown that the morphology of coatings depends on substrate porosity parameters that are optimal for efficient hydrogen-evolving porous coatings are presented.

DOI: 10.1134/S1063784220030251

INTRODUCTION

The search for and development of cheap and reliable cathode materials is currently a topical problem [1]. The primary property of such cathodes is catalytic activity [2]. Nickel and its compounds are cheaper than materials containing noble metals (Pt, Pd), are more abundant in nature, and offer good catalytic activity and high corrosion resistance. Because of this, they have found wide application as cathodes in laboratory and space-borne devices for hydrogen evolution [3–12].

The efficiency of hydrogen evolution and, as a result, the amount of evolved hydrogen depend not only on cathode material but also on active surface area [13–15]. Materials with a well-developed surface usually have a large surface area. For example, we showed earlier that porous anodic alumina (PAA) can be successively used as a coating with a well-developed surface for different materials [16–18]. Under certain preparation conditions, the parameters of PAA (pore diameter, center distance between pores, thickness of walls between pores [19]) are typical of a hexagonally ordered porous structure and may vary over wide limits depending on synthesis conditions [20].

Over the last 10–15 years, various teams of scientists investigated nickel nanostructures obtained using PAA. Specifically, electrodeposited nickel nanostructures were studied in [21–23]. It should be noted however that the use of such structures as cathodes for electrolysis in alkaline electrolytes is inappropriate, since the PAA matrix dissolves in alkalies and the electrode degrades. Using thermal deposition or magnetron sputtering of coatings, one can obtain not only a well-developed surface with a morphology governed

by the surface structure of the porous matrix but also protect the surface against cracking [16, 17]. As a consequence, electrodes with such a coating may be in use sufficiently long. Therefore, the goal of our study was to collect structural, morphological, and electron spectroscopic data for nickel coatings applied by magnetron sputtering on the surface of PAA with different porosity before and after hydrogen evolution reactions.

1. EXPERIMENTAL

PAA films were applied by one-stage anodic deposition [24]. High-purity (99.99%) aluminum sheets measuring $25 \times 25 \times 0.5$ mm were preannealed in air in a muffle furnace at 450°C for 12 h to relieve mechanical stresses and increase grain size. Then, the sheets were electrochemically mirror-polished in a solution of chromium VI oxide (CrO_3 , 185 g/L) and phosphorous acid H_3PO_4 (1480 g/L) kept at 80°C . After that, the sheets were successively rinsed in an ultrasonic acetone bath and in distilled water. Anodizing was carried out by a two-electrode cell filled with a 0.3 M solution of oxalic acid $(\text{COOH})_2$ at a fixed voltage (40, 80, 120 V). A stainless steel wire was used as a cathode. During anodizing, the electrolyte was stirred and its temperature was kept accurate to $2\text{--}4^\circ\text{C}$. Since the anodizing rate is voltage-dependent [19], porous films about $50 \mu\text{m}$ thick were prepared by anodizing initial sheets for 24 h at 40 V (samples AAO_40), (ii) 12 h at 80 V (samples AAO_80), and (iii) 8 h at 120 V (samples AAO_120).

Nickel coatings were deposited in a VUP-5 universal vacuum station equipped with a MAG-2000 dc

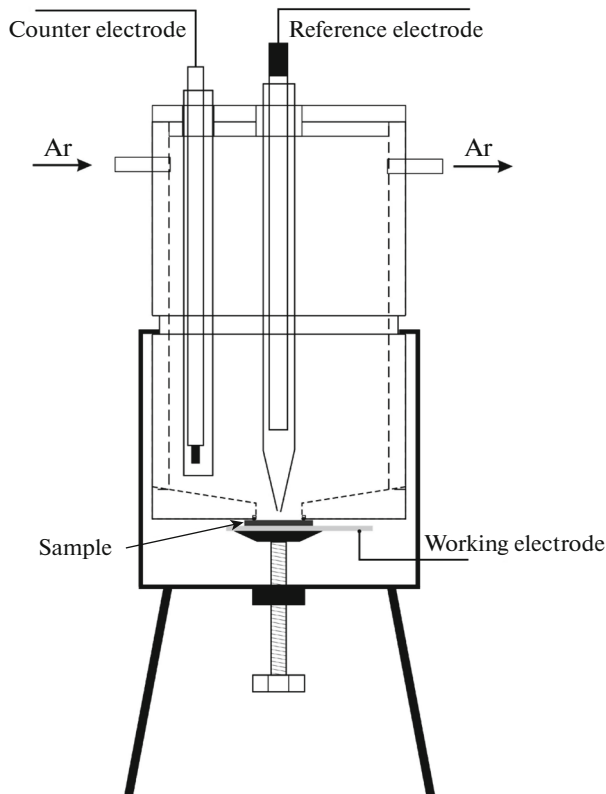


Fig. 1. Electrochemical cell.

magnetron sputtering system 50 mm in diameter (PROTON MIET Co.) Nickel targets (99.99% pure GIRMET), 3 mm in thickness, were applied. Coatings were deposited cyclically (20 cycles, 5 min each) at a magnetron current of 150 mA. In between cycles the magnetron was water-cooled for 10 min. The thickness of deposited coatings was measured interferometrically on a witness sample applied on glass. It was equal to $1.2 \pm 0.1 \mu\text{m}$. The resistivity of all coatings, which was measured by the two-point probe method, was low (less than $10 \Omega/\text{cm}^2$).

The structural state was identified by the X-ray diffraction method in the scan range $2\theta = 30^\circ\text{--}120^\circ$ (CoK_α radiation) with a step of 0.05° using a Rigaku MiniFlex500 diffractometer (Japan).

The chemical composition and electron structures of coatings were examined by X-ray photoelectron spectroscopy (XPS) using a SPECS spectrometer (Germany). Spectra were excited by AlK_α radiation ($E_{\text{ex}} = 1486.6 \text{ eV}$), and the surface was etched to take concentration profiles by Ar^+ ions at an accelerating voltage of 4 keV and a current of 30 μA . The spectra were processed using the CasaXPS program package. The surface morphology of coatings was examined under an FEI Inspect S50 scanning electron microscope (SEM).

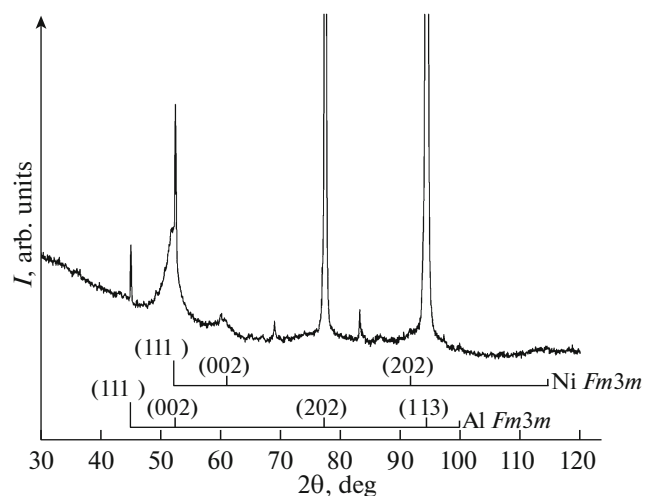


Fig. 2. Typical X-ray diffraction pattern for Ni coatings on porous alumina. Shown also are line diagrams for Ni and Al phase identification.

The cathodic behavior of coatings was studied in a 10% solution of NaHCO_3 (pH 8.7) using an EkoLab 2A-500 potentiometer. A sample (working electrode) was fixed in a three-electrode compression-type cell (Fig. 1) where a platinum electrode was applied as a counter (auxiliary) electrode and an Ag/AgCl electrode was used as a reference one. The solution was aerated by passing argon through a hermetically sealed cell during the experiment.

2. RESULTS AND DISCUSSION

The identification of the nickel coating structure by X-ray diffraction revealed the presence of fcc phases of nickel and substrate aluminum (Fig. 2). Nickel lines are considerably broadened, which indicates a small size of coherent scattering regions.

The SEM micrographs of the porous alumina matrix taken at anodizing voltages of 40, 80, and 120 V (Fig. 3) show that PAA synthesized at voltages of 80 and 120 V, unlike that synthesized at 40 V, has a disordered pore arrangement. The reason is that each electrolyte of a certain composition has its own voltage range in which a well-developed pore structure forms. This is due to limitations imposed on the migration rate of aluminum and oxygen ions in a barrier layer between an electrolyte and a metal [25]. Therefore, to provide an ordered arrangement of pores at anodizing voltages of 80 and 120 V, one has to take an electrolyte of another composition. Since our aim was to obtain coatings with a well-developed surface, the regular arrangement of pores was of minor significance. It should be noted that pores in sample AAO_120 are finer than in sample AAO_80. This is due to the fact that in the case of high anodizing voltages, the voltage was smoothly increased from 0 to 120 V for 1 min to prevent electrical breakdown, which could take place

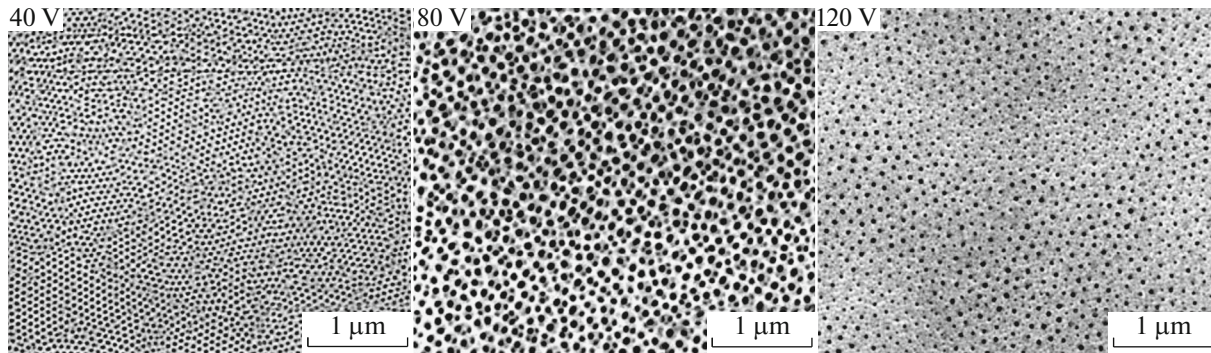


Fig. 3. SEM micrographs of PAA films obtained at anodizing voltages of 40, 80, and 120 V (samples AAO_40, AAO_80, and AAO_120, respectively).

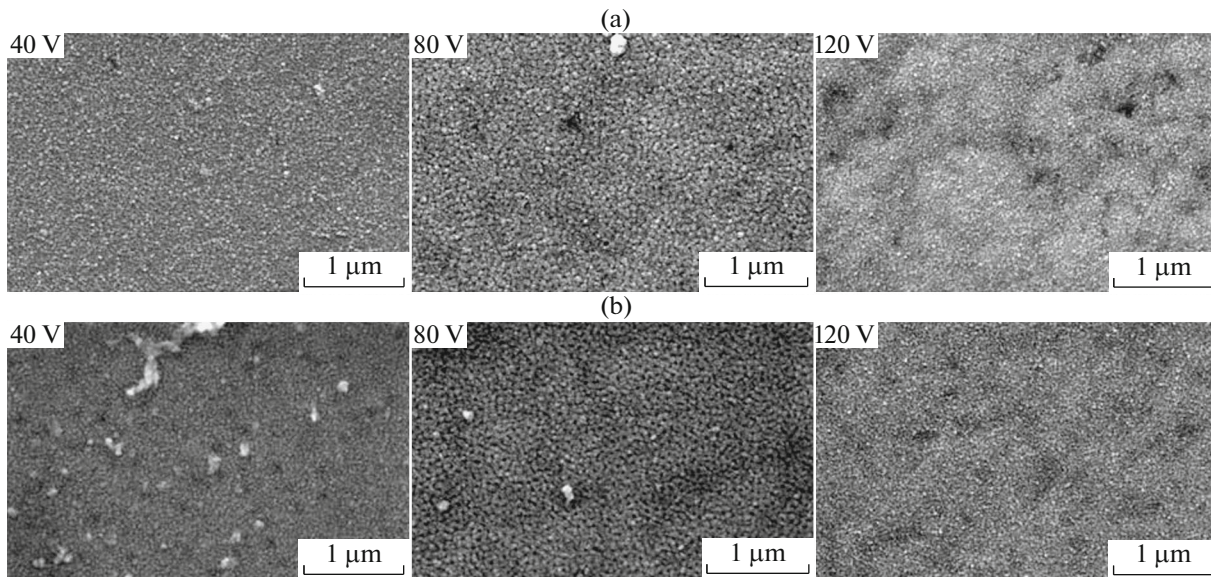


Fig. 4. SEM micrographs taken of the surface of nickel coatings on PAA matrices (a) before and (b) after the cathodic reaction of hydrogen evolution.

at a sharp (stepwise) voltage rise. Since the pore diameter on the surface is rather small, the mean distance between pores corresponds to a value that must be at 120-V anodizing voltage [19].

The SEM micrographs taken of nickel-covered PAA matrices before (Fig. 4a) and after (Fig. 4b) the hydrogen evolution (cathodic) reaction show that matrices formed at 40 and 120 V are covered by coatings made up of nanoparticles with a characteristic size of 30–40 nm, pores in the matrix being completely closed. This suggests that nanoparticles of which coatings form condense in the interporous area of the matrix, step-by-step “healing” the pores. This mechanism activates when the pore size becomes smaller than the thickness of walls between pores (cf. with PAA surface micrographs in Fig. 3) [26]. Coatings on matrices obtained at an anodizing voltage of 80 V seem to form propagating from the boundary of

pores toward their center [26]; however, since the pore diameter is much greater than the thickness of walls between pores (Fig. 3, central part of the PAA micrograph), the nickel surface has a pronounced pore structure on the surface.

The cathodic performance of nickel coatings on PAA matrices versus cathodic polarization curves for nickel films on glass and polished aluminum is shown in Fig. 5. The cathode current value is a measure of hydrogen evolution efficiency: the higher the cathode current, the greater amount of evolved hydrogen with the voltage being the same. Coatings on the AAO_120 matrix demonstrate a maximal cathode current, whereas those on the AAO_40 matrix have a minimal current. The current of coatings on the AAO_80 matrix is slightly lower than that of coatings on the AAO_120 matrix. The difference between cathode currents of AAO_40 and AAO_120 samples is large in

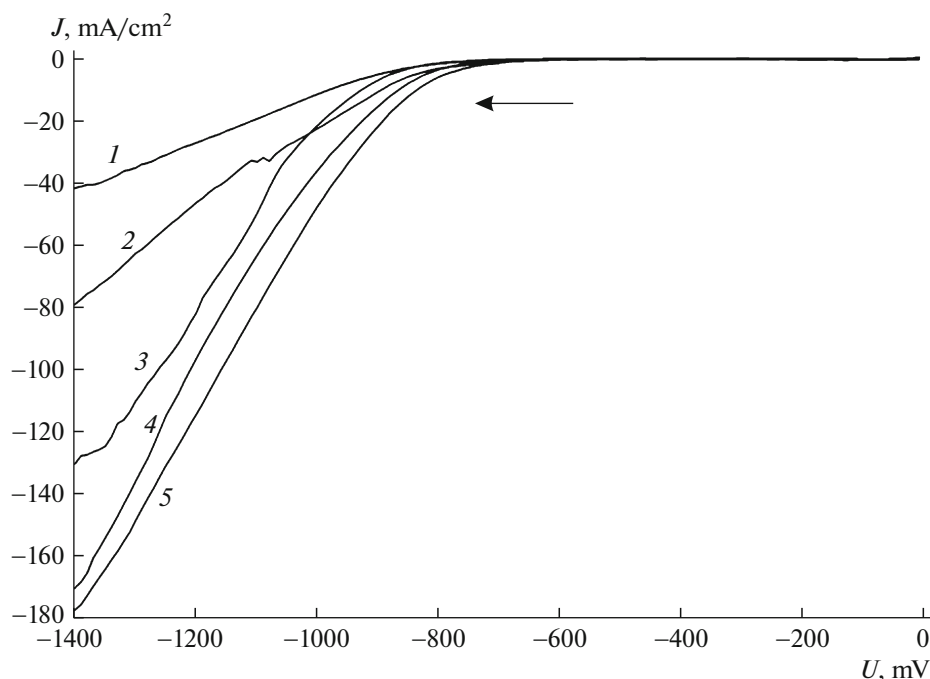


Fig. 5. Cathodic polarization curves for nickel coatings on samples (1) AAO_40, (2) glass, (3) polished aluminum, (4) AAO_80, and (5) AAO_120.

spite of comparable sizes of nanoparticles, which may be associated with different chemical states of nickel on the surface: oxide arising on the AAO_40 surface is thicker, as follows from XPS data.

Different values of current density in films grown on flat surfaces of glass and aluminum can be explained by different contact resistances in the case of cathodic potential application: the contact area between aluminum and the contact pad of the working electrode is greater than that of a jumper connecting the nickel surface and back side of the sample. This is also the reason for why nickel on glass remains incompletely oxidized (Fig. 6d) in contrast to the case of coatings on PAA (Figs. 6a–6c).

As has been mentioned above, XPS data shed light on the chemical state of nickel. From Ni $2p_{3/2}$ spectra (Fig. 6) it follows that before the coating experiences a hydrogen evolution reaction, the spectrum is typical of the nickel surface after its short-term low-temperature oxidation in air. The sample has an ultrathin oxide film with a thickness less than the XPS analysis depth ($E_b \approx 856$ eV), and the spectrum has the line of pure nickel (~ 853 eV). A shake-up satellite peak in the range 861–862 eV is a characteristic sign of chemical state Ni $^{2+}$ of bivalent nickel [27].

After the hydrogen evolution reaction, the metallic nickel component in the spectrum almost disappears: the surface contains mainly nickel compounds with a degree of oxidation of 2+. When the cathode potential, which is initially equal to -0.72 eV relative to the

hydrogen electrode, grows during potentiodynamic studies, Ni(OH) $_2$ hydroxide forms on the nickel surface according to [28]. It is not surprising, since in the course of the cathodic reaction of electrolysis, water molecules dissociate into hydrogen ions H $^+$, which combine near a catalytic surface to form hydrogen gas and hydroxyl ions (OH) $^-$, which oxidize the nickel surface. Nickel is reduced during the back reaction at the same potential.

After the cathodic reaction was completed, we took spectra from the etched surface. The surface was etched by 1-keV Ar $^+$ ions. From these spectra, we managed to compare the thicknesses of resulting Ni $^{2+}$ -based layers using the metal nickel-to Ni $^{2+}$ ion intensity ratio. It is seen that this intensity ratio is the least and the greatest in the spectra taken of coatings on the AAO_40 and AAO_120 matrices, respectively. This agrees well with maximal current values in cathode polarization curves. In other words, nickel on the AAO_40 surface oxidizes more rapidly, as a result of which the resistivity of samples and, as a consequence, the cathodic current drop.

CONCLUSIONS

Based on experimental data for nickel coatings magnetron sputtered on a well-developed PAA surface, the following conclusions can be drawn.

(i) Depending on the matrix (substrate) morphology, either crystalline fcc nickel coatings consisting of

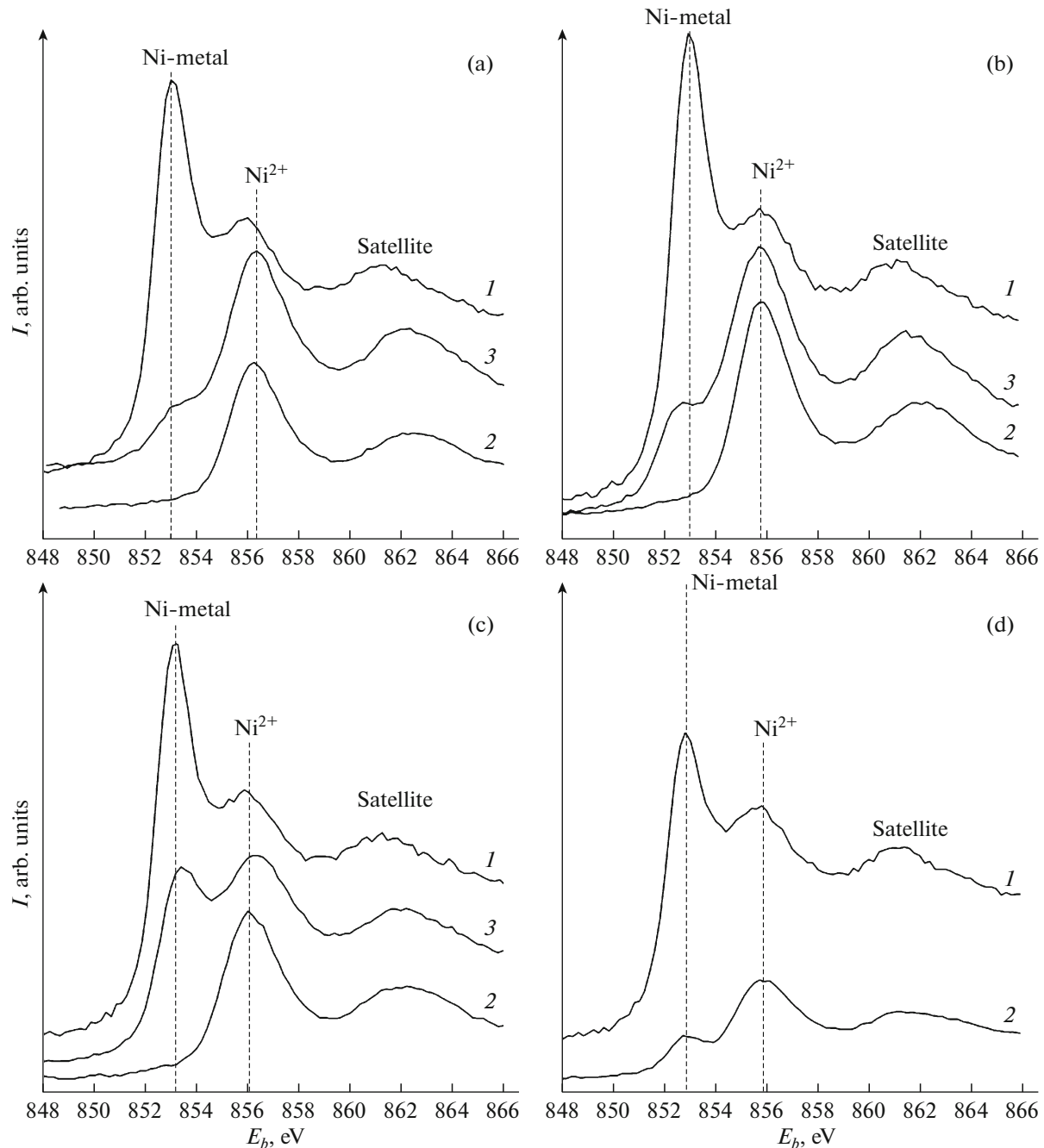


Fig. 6. XPS spectra of $\text{Ni}2p_{3/2}$ for Ni coatings (1) before the cathodic reaction, (2) after the cathodic reaction, and (3) after the cathodic reaction and subsequent surface etching by 1-keV Ar^+ ions for 1 min: (a) AAO_40 matrix, (b) AAO_80 matrix, (c) AAO_120 matrix, and (d) glass substrate.

nanoparticles 30–40 nm across (AAO_40 and AAO_120 matrices) or porous nickel films duplicating the substrate porosity (AAO_80) form. This is associated with different coating formation mechanisms on Al_2O_3 substrates with different pore diameter-to-pore distance ratios.

(ii) Coatings on AAO_80 and AAO_120 matrices demonstrate the highest efficiency of the hydrogen

evolution cathodic reaction (the highest current density) at a cathode potential of -1.4 V.

(iii) After the cathodic reaction is completed, the nickel surface is completely oxidized to nickel state Ni^{2+} . The thickness of the oxidized layer is maximal in samples with a low efficiency of hydrogen evolution (coating on the AAO_40 matrix) and minimal in the sample with the highest cathodic efficiency (coating on the AAO_120 matrix).

ACKNOWLEDGMENTS

The authors thank V.A. Volkov (Udmurt Federal Research Center, Ural Branch, Russian Academy of Sciences) for assistance in conducting X-ray diffraction analysis.

FUNDING

This study was performed using the equipment of the Center of Physical and Physicochemical Methods to Study the Properties and Characteristics of Surface, Nanostructures, Materials, and Product (Udmurt Federal Research Center, Ural Branch, Russian Academy of Sciences) as part of the program for basic research (Ural Branch, Russian Academy of Sciences, project no. 18-10-2-25) and project no. AAAA-A17-117022250040-0 of the Surface Physics and Chemistry Department of the Udmurt Federal Research Center.

CONFLICT OF INTEREST

The authors claim that there are no conflicts of interest.

REFERENCES

- O. Schmidt, A. Gambhir, I. Staffell, A. Hawkes, J. Nelson, and S. Few, *Int. J. Hydrogen Energy* **42**, 30470 (2017). <https://doi.org/10.1016/j.ijhydene.2017.10.045>
- S. Aouad, M. Labaki, S. Ojala, P. Seelam, E. Turpeinen, C. Gennequin, J. Estephane, and E. Abi Aad, in *Catalytic Materials for Hydrogen Production and Electrooxidation Reactions*, Ed. by M. R. Cesario, C. Gennequin, E. Abi-Aad, and D. A. de Macedo (Bentham Science, 2018), pp. 60–128. <https://doi.org/10.2174/97816810875801180201>
- J. O'M. Bockris and E. C. Potter, *J. Chem. Phys.* **20**, 614 (1952). <https://doi.org/10.1063/1.1700503>
- J.-Y. Huot, *J. Electrochem. Soc.* **136**, 1933 (1989). <https://doi.org/10.1149/1.2097088>
- M. Gong, W. Zhou, M.-C. Tsai, J. Zhou, M. Guan, M.-C. Lin, B. Zhang, Y. Hu, D.-Y. Wang, J. Yang, S. J. Pennycook, B.-J. Hwang, and H. Dai, *Nat. Commun.* **5**, 4695 (2014). <https://doi.org/10.1038/ncomms5695>
- D. Stolten, *Hydrogen Science and Engineering: Materials, Processes, Systems and Technology* (Wiley, 2016).
- M. Schalenbach, F. D. Speck, M. Ledendecker, O. Kasian, D. Goehl, A. M. Mingers, B. Breitbach, H. Springer, S. Cherevko, and K. J. J. Mayrhofer, *Electrochim. Acta* **259**, 1154 (2018). <https://doi.org/10.1016/j.electacta.2017.11.069>
- C. Lupi, A. Dell'Era, and M. Pasquali, *Int. J. Hydrogen Energy* **34**, 2101 (2009). <https://doi.org/10.1016/j.ijhydene.2009.01.015>
- M. H. Tang, C. Hahn, A. J. Klobuchar, J. Wei, D. Ng, J. Wellendorff, T. Bligaard, and T. F. Jaramillo, *Phys. Chem. Chem. Phys.* **16**, 19250 (2014). <https://doi.org/10.1039/c4cp01385a>
- S. Saha, S. Vaidya, K. V. Ramanujachary, S. E. Lofland, and A. K. Ganguli, *Bull. Mater. Sci.* **39**, 433 (2016).
- H. Yamashita, T. Yamamura, and K. Yoshimoto, *J. Electrochem. Soc.* **140**, 2238 (1993). <https://doi.org/10.1149/1.2220802>
- A. R. J. Kucernak and V. N. N. Sundaram, *J. Mater. Chem. A* **2**, 17435 (2014). <https://doi.org/10.1039/c4ta03468f>
- X. Zhang, J. Hampshire, K. Cooke, X. Li, D. Pletcher, S. Wright, and K. Hyde, *Int. J. Hydrogen Energy* **40**, 2452 (2015). <https://doi.org/10.1016/j.ijhydene.2014.12.107>
- I. Herraiz-Cardona, C. González-Buch, E. Ortega, J. García-Antón, and V. Pérez-Herranz, *Chem. Eng. Trans.* **32**, 451 (2013). <https://doi.org/10.3303/CET133076>
- C. González-Buch, I. Herraiz-Cardona, E. Ortega, J. García-Antón, and V. Pérez-Herranz, *Chem. Eng. Trans.* **32**, 865 (2013). <https://doi.org/10.3303/CET1332145>
- R. G. Valeev, V. V. Stashkova, A. I. Chukavin, V. A. Volkov, A. S. Alalykin, A. V. Syugaev, A. N. Beltiukov, F. Z. Gil'mutdinov, V.V. Kriventsov, and N. A. Mezentsev, *Phys. Proc.* **84**, 407 (2016). <https://doi.org/10.1016/j.phpro.2016.11.069>
- R. G. Valeev, A. L. Trigub, A. N. Beltiukov, D. I. Petukhov, I. A. El'kin, and V. V. Stashkova, *J. Surf. Invest.: X-Ray, Synchrotron Neutron Tech.* **13**, 92 (2019). <https://doi.org/10.1134/S1027451019010373>
- R. G. Valeev and A. S. Alalykin, *Proc. LIII School on Condensed State Physics, St. Petersburg, Russia, 2019*, p. 88.
- D. I. Petukhov, R. G. Valeev, and S. M. Reshetnikov, *Porous Anode Aluminum and Titanium Oxides: Structure, Properties, Synthesis* (Udmurt. Univ., Izhevsk, 2018).
- I. V. Roslyakov, A. A. Eliseev, E. V. Yakovenko, A. V. Zabelin, and K. S. Napolskii, *J. Appl. Crystallogr.* **46**, 1705 (2013). <https://doi.org/10.1107/S002188981302579X>
- K. S. Napolskii, A. A. Eliseev, N. V. Yesin, A. V. Lukashin, Yu. D. Tretyakov, N. A. Grigorieva, S. V. Grigoriev, and H. Eckerlebe, *Phys. E* **37**, 178 (2007). <https://doi.org/10.1016/j.physe.2006.08.018>
- M. P. Proenca, C. T. Sousa, J. Ventura, M. Vazquez, and J. P. Araujo, *Electrochim. Acta* **72**, 215 (2012). <https://doi.org/10.1016/j.electacta.2012.04.036>
- Y. Yu, J. Li, J. Wang, X. Wu, C. Yu, T. Xu, B. Chang, H. Sun, and H. Arandiyani, *Catalysts* **9**, 152 (2019). <https://doi.org/10.3390/catal9020152>
- H. Masuda and M. Satoh, *Jpn. J. Appl. Phys.* **35**, L126 (1996). <https://doi.org/10.1143/JJAP.35.L126>
- K. S. Napolskii, I. V. Roslyakov, A. A. Eliseev, D. V. Byelov, A. V. Petukhov, N. A. Grigorieva, W. G. Bouwman, A. V. Lukashin, A. P. Chumakov, and S. V. Grigoriev, *J. Phys. Chem. C* **115**, 23726 (2011). <https://doi.org/10.1021/jp207753v>
- R. Valeev, A. Beltiukov, V. Mukhgalin, and R. Zakirova, *Mater. Res. Express* **3**, 015902 (2016). <https://doi.org/10.1088/2053-1591/3/1/015902>
- C. D. Wagner, W. M. Riggs, L. E. Davis, J. F. Moulder, and G. E. Muilenberg, *Handbook of X-Ray Electron Spectroscopy* (Perkin-Elmer, 1979).
- Handbook on Electrochemistry*, Ed. by A. M. Sukhotin (Khimiya, Leningrad, 1981).

Translated by V. Isaakyan